The *vestigial* Quadrant Enhancer is dispensable for pattern formation and development of the *Drosophila* wing

Keity J Farfán-Pira[1], Teresa I Martínez-Cuevas[1], Rosalio Reyes[1], Timothy A Evans[2], Marcos Nahmad[1§]

[1]Department of Physiology, Biophysics, and Neurosciences, Centre for Research and Advanced Studies of the National Polytechnic Institute (Cinvestav-IPN)

[2]Department of Biological Sciences, University of Arkansas

[§]To whom correspondence should be addressed: mnahmad@fisio.cinvestav.mx

Abstract

In *Drosophila*, the pattern of the wing selector gene, *vestigial* (*vg*), is established by at least two enhancers: the Boundary Enhancer, which drives expression along the disc's Dorsal-Ventral boundary; and the Quadrant Enhancer (QE) that patterns the rest of the wing pouch. Using CRISPR/Cas9 editing, we deleted DNA fragments around the reported QE sequence and found that the full Vg pattern is formed. Furthermore, adult wings arising from these gene-edited animals are normal in shape and pattern, but slightly smaller in size, although this reduction is not wing-specific in males. We suggest that other enhancers act redundantly to establish the *vg* pattern and rescue wing development.

A.

B. *vg*ΔQE+SID   *vg*ΔQE   *vg*ΔCTRL

C. Females   Males

D. Females   Males

E. Females   Males
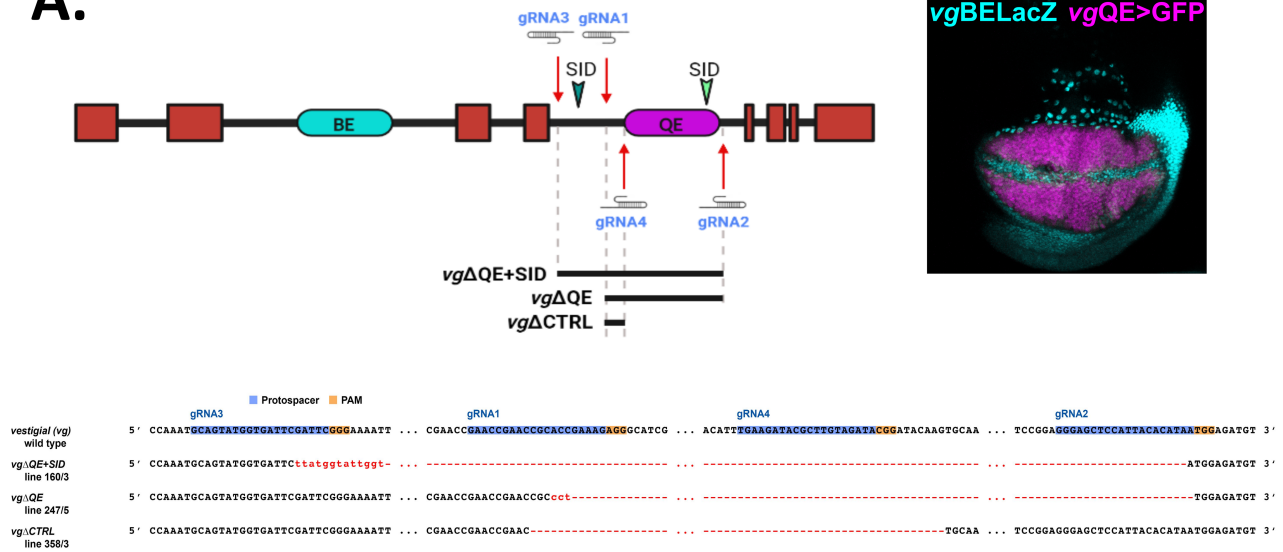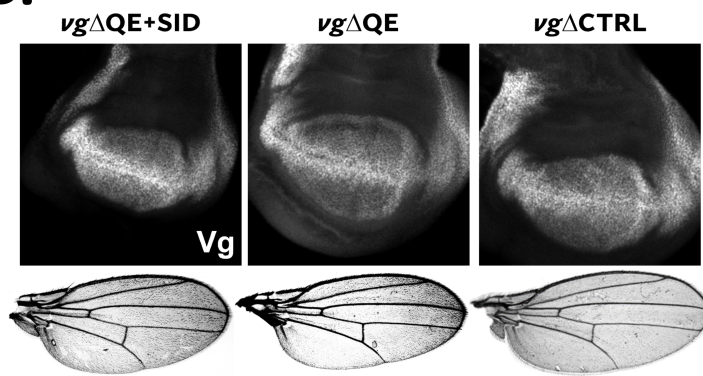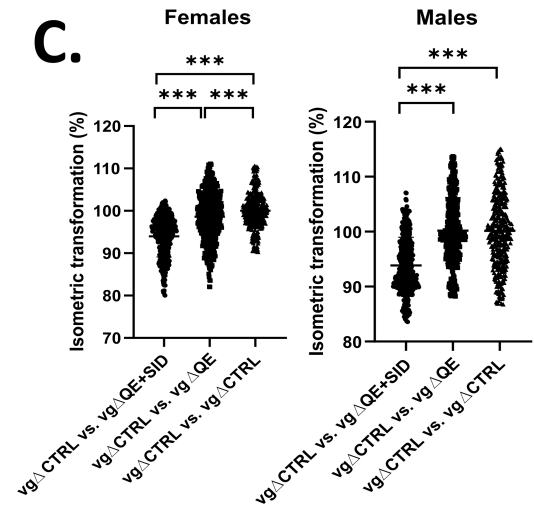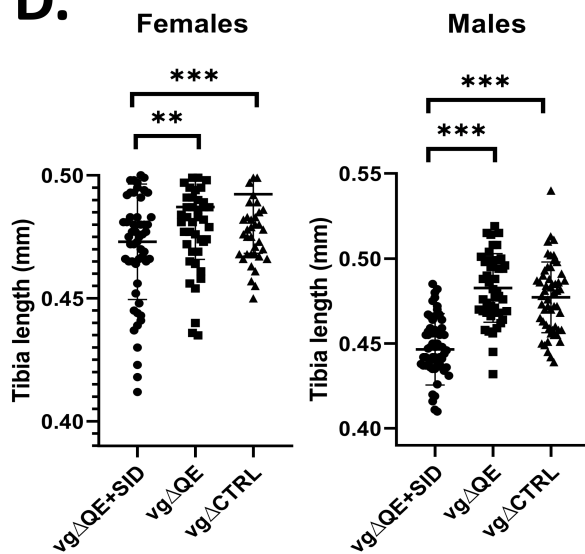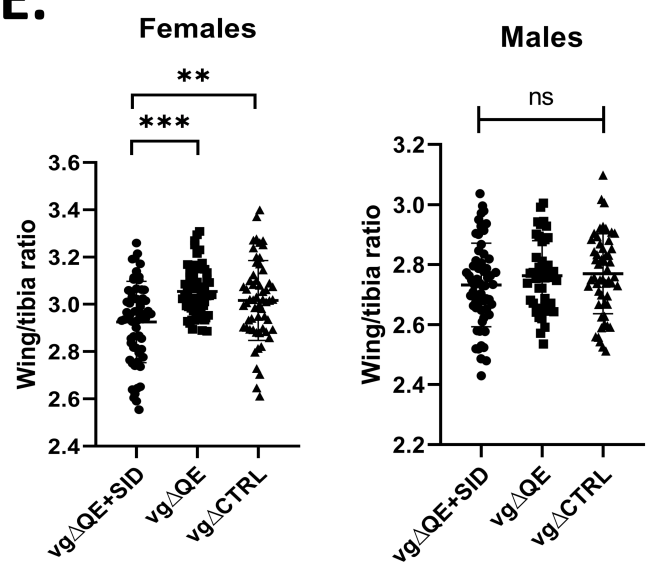
Figure 1. Vg patterning and adult wing development is largely unaffected in CRISPR-edited animals that lack the QE sequence.

(A) Scheme of the *vg* gene showing the two intronic enhancers (BE, Boundary Enhancer; QE, Quadrant Enhancer) that account for the full Vg pattern in the third-instar wing imaginal disc (photo in the right: vgBELacZ=reporter of the BE marked by βGal immunostaining; vgQE>GFP=reporter of the QE marked by GFP expression under the Gal4-UAS system). The location of gRNAs (marked by red arrows) that were used to delete different fragments (black bars) within the fourth intron that contains the QE are shown: *vg*ΔQE+SID (gRNA3 and gRNA2, that contains an additional SID (green arrowhead) outside of the reported QE element), *vg*ΔQE (gRNA1 and gRNA2), or *vg*ΔCTRL. The sequencing results confirming each of the CRISPR/Cas9 deleted elements are shown; gRNAs protospacers (highlighted in blue) and PAM sites (highlighted in orange) are illustrated; sequence mismatches are displayed in red font. **(B)** Photos of representative wing imaginal discs displaying late third-instar larvae immunostained with Vg and female adult wings for each of the CRISPR/Cas9 edited lines. **(C)** Pairwise comparison of control *vs*. QE-deleted wings. An isometric transformation is applied to each control wing to match an experimental wing and the isometric transformation factor (in %) is plotted. Female and male wings are independently compared. Groups that are statistically significant after a one-way ANOVA analysis are shown. **(D, E)** Comparison of anterior tibia lengths (D) and wing to tibia length ratios (E) in each of the CRISPR/Cas9 edited lines. Female and male animals are independently compared. Groups that are statistically significant after a one-way ANOVA analysis are shown. (**:p-value<0.005; ***:p-value<0.0005; ns: not statistically-significant).

Description

Activation of gene expression during development is controlled by enhancers, which are DNA sequences that contain transcription factor binding sites and drive the recruitment of the transcriptional machinery in a context-specific manner (Field & Adelman, 2020; Furlong & Levine, 2018; Long et al., 2016). Complex developmental patterns often require the action of one or multiple enhancers, which are precisely coordinated in space and time. Sometimes, two or more *cis*-regulatory elements establish an overlapping pattern of gene expression and they are referred as shadow enhancers (Hong et al., 2008). Shadow enhancers appear to be widespread in metazoan genomes suggesting that their role may be evolutionary conserved to confer robust gene expression patterns under genetic or environmental perturbations (Kvon et al., 2021).

In *Drosophila*, wing fate is determined by the expression of the selector gene, *vestigial* (*vg*), which is confined to an area within the wing imaginal disc referred as the wing pouch (Kim et al., 1996; Williams et al., 1991; Williams et al., 1993). The *vg* pattern is established by two intronic enhancers: the Margin or Boundary Enhancer (BE), and the Quadrant Enhancer (QE; Fig. 1A). Early in wing disc development, the BE drives *vg* expression in cells abutting the Dorsal-Ventral (DV) boundary (cyan staining, Fig. 1A) in response to a short-range Delta/Serrate-Notch and Wingless (Wg) signaling (Couso et al., 1995; de Celis et al., 1996; Doherty et al., 1996; Irvine & Vogt, 1997; Kim et al., 1995; Williams et al., 1994). As these Vg-expressing cells proliferate, they leave the DV signaling center, but maintain *vg* expression presumably through Polycomb/Trithorax Responsive Elements (PRE) and Vg autoregulation (Ahmad & Spens, 2019; Halder et al., 1998; Klein & Arias, 1999; Pérez et al., 2011; Simmonds et al., 1998). In addition, the QE drives *vg* expression in the rest of the wing pouch through the integration of several signaling networks including the long-range action of the Wg and Decapentaplegic (Dpp) morphogens (Kim et al., 1996; Klein & Arias, 1998; Lecuit & Cohen, 1998; Nellen et al., 1996; Neumann & Cohen, 1996; Zecca et al., 1996) and a Fat/Dachsous polarization signal that results in the recruitment of Vg in neighboring cells (Zecca & Struhl, 2007a; Zecca & Struhl, 2007b; Zecca & Struhl, 2010). At the transcriptional level, the recruitment signal depends on the nuclear translocation of Yorkie (Yki), the effector of the Warts-Hippo tumor suppressor pathway, which binds the TEAD-transcription factor Scalloped (Sd) and activate *vg* expression through Scalloped-Interaction Domains (SIDs) (Simmonds et al., 1998; Zecca & Struhl, 2010). A bioinformatic analysis reveals two SIDs within the fourth intron of the *vg* gene; one within the reported QE sequence (Klein & Arias, 1999; Williams et al., 1994; Zecca & Struhl, 2007a) and another one located 544 base pairs upstream of it (Fig. 1A).

Transgenic reporters show that the QE can drive *vg* expression in most of the wing pouch (magenta staining, Fig. 1A), but it is unknown whether or not the QE is necessary for *vg* expression and wing development. In order to investigate this, we designed guide RNAs (gRNAs) to delete the reported QE (*vg*ΔQE; using gRNA1 and gRNA2, Fig. 1A) or the reported QE plus the additional SID (*vg*ΔQE+SID; using gRNA3 and gRNA2, Fig. 1A) using CRISPR/Cas9 Non-Homologous End-Joining (NHEJ) technology (see Methods; Evans, 2017; Port et al., 2014). As a control, we deleted a small piece of DNA that does not overlap with the reported QE sequence nor contains a SID (*vg*ΔCTL; using gRNA1 and gRNA4; Fig. 1A). However, none of these deletions have an effect in the Vg pattern of late third-larval wing discs, which appears to cover all the wing pouch, nor in the shape and pattern of the adult wing (Fig. 1B). We did notice a minor, albeit significant reduction in wing size of the *vg*ΔQE+SID line in both males and females with respect to the other deletions (Fig. 1C). Strikingly however, this reduction is not specific to the wing, as measurements of anterior legs' tibias are also significantly smaller in *vg*ΔQE+SID

animals with respect to the other lines, especially in males (Fig. 1D). In fact, when each wing measurement is normalized to the length of the corresponding tibia (wing to tibia ratio), we found that the size difference only persist in females (Fig. 1E), suggesting that *vg*ΔQE+SID males are proportionally smaller. These results highlight the potential impact of the additional SID on size control. Taken together, our data suggest that the QE is not required for Vg nor wing patterning, except for small sex-specific effects in animal size that occur only with an additional SID is deleted. However, we cannot rule out that Vg expression levels or its dynamics may be affected by the deletions.

Given the importance of Vg expression for wing differentiation, other regulatory elements may ensure that animals develop fully functional wings upon genetic mutations in the QE. This suggests the existence of shadow enhancers within the *Drosophila* genome that rescue the Vg pattern in the absence of the QE. These shadow enhancers likely respond to the same signaling pathways since the Vg pattern does not expand without these signals (Zecca & Struhl, 2007b). In addition, our data reveal the potential impact of SIDs on animal size. How could a regulatory sequence within the wing selector gene have an effect in the overall size of an animal? One possibility is that SIDs affect overall size through Yki-Sd binding, which is known to promote cell growth and/or proliferation in a plethora of systems (Goulev et al., 2008; Hariharan, 2015; Huang et al., 2005; Wu et al., 2008). Alternatively, perhaps the *vg*ΔQE+SID deletion affects size in a wing-specific manner and inter-organ coordination of size is established through systemic signals (Boulan et al., 2019; Colombani et al., 2012; Mesquita et al., 2010). Another interesting finding to explore in future work is the sex-specific wing *vs.* overall size difference (Fig. 1D,E). Since the *sd* gene is located in the first chromosome (Dmel\sd, FlyBase ID FBgn0003345), it is plausible that males and females respond differently to SID deletions. Finally, since *vg* is an evolutionary-conserved wing selector gene in insects (Abouheif & Wray, 2002; Clark-Hachtel et al., 2013; Clark-Hachtel et al., 2021; Zhang et al., 2021), our work highlights the impact of CRISPR/Cas9 editing to understand the contribution of regulatory elements to wing diversity (Medved et al., 2015; Linz & Tomoyasu, 2018).

Methods

gRNA Design

Target sites were designed using flyCRISPR online tool CRISPR Optimal Target Finder (https://flycrispr.org) (Iseli et al., 2007; Gratz et al., 2014).

Construction of gRNA plasmid

Cloning was performed using pCFD4-U6:1_U6:3tandemgRNAs vector, that allows in-tandem expression of gRNA sequences (Port et al., 2014; Evans, 2017), through PCR products using pair of primers 1 and 2, 2 and 3, 1 and 4, and 3 and 4 (see Reagents), amplified with 2X Phusion Flash PCR Master Mix. Gibson Assembly was performed with PCR products and pCFD4 *Bbs*I digested vector. Clonings was confirmed by Sanger sequencing by Eurofins Genomics prior to injection.

Identification of CRISPR-modified alleles

The vg^{QE} gRNA plasmid was injected into *nos*-Cas9 embryos by Best Gene (Chino Hills, CA). Injected individuals (G0) were crossed as adults to *Sco/CyoRFP*. Founders (G0 flies producing F1 progeny carrying modified QE alleles) were identified using pools of three females derived from each G0 cross by PCR with primers 5 and 12 (for *vg*ΔQE+SID) or 12 and 13 (for *vg*ΔQE and *vg*ΔCTRL) which produce 0.5-kb or 1.5-kb respectively when the respective NHEJ (Non-Homologous End Joining) are present. From each identified founder, 5-10 F1 males were then crossed individually to *Sco/CyORFP* virgin females. After 3 days, F1 males were removed from the crosses and tested by PCR with the same set of primers to verify if they carried the modified allele. F2 flies from F1 crosses were used to generate balanced stocks, and the modified alleles were sequenced from genomic DNA using primers 12, 18 and 13 (see Reagents).

Fly stocks and wing imaginal disc immunostaining

The disc shown in Fig. 1A was obtained by crossing flies carrying a transgenic reporter of the vg BE in the second chromosome (vgBElacZ [obtained from Marco Milán]) with flies expressing nuclear GFP under the Gal4-UAS system (vgMQGal4 / SM6; UAS-GFP$_{nls}$ / TM6B, Tb). For the immunostaining, wandering third-instar larvae were dissected in PEM (Na-Pipes 80mM + EGTA 5mM) solution. The internal tissue of anterior part was exposed with independent needles and larvae were fixed in 4% paraformaldehyde solution during 40 minutes at room temperature. Dissected larvae were then washed three times in PEM-T solution (PEM + Triton X100) in agitation for 10 minutes. Subsequently, samples were incubated with a blocking solution that contains PEM-T and 0.5% Bovine Serum Albumin (BSA), for two hours in agitation at room temperature. Blocking solution was discarded and primary antibodies were added (mouse anti-βGalactosidase at 1:1000 in Fig. 1A [no antibody was needed to detect GFP]; and Guinea-pig anti-Vg [kindly provided by Gary Struhl] at 1:200 in Fig. 1B) in staining solution (blocking solution + 1% Normal Goat Serum) and incubated overnight at 4 °C.

Primary antibodies were recovered, and the sample was washed three times with PEM-T solution at room temperature for 10 minutes. Incubations with secondary antibodies were performed with Alexa Fluor 647 anti-mouse (Fig. 1A) and Alexa Fluor 594 anti-Guinea Pig (Fig. 1B) at a concentration of 1:1000 each for two hours at room temperature in the dark. The sample was washed once again three times with PEM-T solution and one time with PEM solution for 10 minutes at room temperature in the dark. Discs were dissected and mounted using a stereoscopic microscope (Nikon SMZ800) in 15 µl of Mowiol solution.

Confocal microscopy and image capture

Imaginal wing disc micrographs were taken using a Spectral confocal microscope (Leica TCS-SP8) using a 63x objective (PL APO CS2, 63x, App. Num. 1.4 oil immersion) and the following specifications in LAS X software: Format 1024 x 1024, speed 600, Frame average 4, Phase X -33.48, Zoom factor 1.00, Z-step size 0.50, Smart gain 776.8 V, Smart offset -3.0% and Pinhole 1 AV. The images were stored in ".lif" format and subsequently analyzed with ImageJ software (https://imagej.nih.gov/ij/download.html) (Schneider et al., 2012). Values and statistical analysis were plotted in GraphPad Prism version 8.0.1.

Isometric transformation

Using Python (3.7.6), we developed a code that given two numpy arrays of the same length (referred with the sub-index 1 and 2):

1. Standardizes the two arrays in such a way the centroid of each array is brought to the origin of coordinates.

2. Returns the isometric transformation factor (Fig. 1C), that minimizes the sum:

$$\Sigma(x_{1i}-\mu x_{2i})^2 + (y_{1i} - \mu y_{2i})^2$$

where (x_{1i}, y_{1i}) are the coordinates of the i-th point of the standardized array 1 and µ is the contraction factor. These points are selected to be the intersection between each vein or intervein with each other or with the wing margin.

Wing/tibia measures

Adult flies of *vg*ΔQE+SID, *vg*ΔQE, and *vg*ΔCTRL lines were separated by sex, using a stereoscopic microscope (Nikon SMZ800) and preserved in 1ml 70% ethanol for dehydration for 12 hours. Each specimen was dissected in 15µl of 50% ethanol to obtain each pair of wings the corresponding pair of front legs mounted in microscope slides.

Wings and legs were photographed in a binocular microscope (Nikon Eclipse Ci) attached to a camera (ProgRes® CT5, Jenoptik) to allow measures (in wings, length of area between veins L3 and L4; in legs, length of tibia), using the ProgRes® Capture Pro-2.9 software. Measurements were performed using ImageJ software 1.53c (Wayne Rasband, National Institutes of Health, USA) using corresponding calibration for 4X objective (Distance in pixels: 100.501; known distance: 0.1; pixel aspect ratio: 1.0, unit of length: mm). Ratio of each wing to tibia proximal distal length were plotted using GraphPad Prism version 8.0.1.

Statistical analysis

A one-way ANOVA was performed to compare the wing to tibia ratios of each of the fly lines generated through CRISPR, with α =0.05. Subsequently, to establish the significant differences between groups, Tukey's range test was performed with α = 0.05.

Reagents

REAGENT	SOURCE	IDENTIFIER
PIPES sodium salt	Sigma-Aldrich	Sigma Prod. No. P2949
EGTA Ethylene glycol-bis(2-amino-ethylether)-N,N,N',N'-tetraacetic acid	Sigma-Aldrich	Sigma Prod. No. E3889
Triton X-100	Sigma-Aldrich	Sigma Prod. No. T9284

8% paraformaldehyde	Electron Microscopy Science	Cat. # 157-8
Bovine Serum Albumin BSA	Sigma-Aldrich	Sigma Prod. No. A2058
Normal Goat Serum	Invitrogen	Catalog # 31872

GENOTYPE	AVAILABLE FROM
vgBElacZ (II)	Marco Milán
vgMQGal4;UAS-GFPnls	Bloomington Drosophila Stock Center, Stocks #8230 and #4776
*vg*ΔQE+SID	This study
*vg*ΔQE	This study
*vg*ΔCTRL	This study
yw;nos-Cas9(III-attP2)/TM6,Tb,Sb	NIG-FLY # CAS-0012
w; Sco/CyO-RFP	Generated in Evans laboratory

PLASMID	GENOTYPE	DESCRIPTION
pCFD4	pCFD4-U6:1_U6:3tandemgRNAs	Addgene plasmid # 49411; http://n2t.net/addgene:49411; RRID: Addgene_49411

ANTIBODY	ANIMAL AND CLONALITY / SOURCE	DESCRIPTION
Anti-Vestigial	Guinea pig polyclonal	Kindly provided by Gary Struhl (Columbia University)
Anti-β-Galactosidase	Mouse polyclonal, Promega	Catalog #Z378A
Alexa Fluor 594 goat anti-Guinea Pig IgG (H+L)	Thermo Fisher Scientific	Catalog # A-11076
Alexa Fluor 647 goat anti-Mouse IgG (H+L)	Thermo Fisher Scientific	Catalog #A-21236

OLIGO 5'-3'	NAME	SEQUENCE

1	QE5'	GGAAAGATATCCGGGTGAACTTCGAACCGAACCGCACCGA AAGGTTTTAGAGCTAGAAATAGCAAG
2	QE3'	GCTATTTCTAGCTCTAAAACTTATGTGTAATGGAGCTCCC GACGTTAAATTGAAAATAGGTC
3	TEA2	GGAAAGATATCCGGGTGAACTTCGCAGTATGGTGATTCGA TTCGTTTTAGAGCTAGAAATAGCAAG
4	Neg	GCTATTTCTAGCTCTAAAACTATCTACAAGCGTATCTTCC GACGTTAAATTGAAAATAGGTC
5	LHA1- F	ACATGCATGCATGTGGAAATGCCACCACTTTGTGCG
12	RHA3-R	CCGCTCGAGGAAATCGCGCGACGCCGCC
13	LHA RecSp-F	CGCGGATCCCTAGTTGGAATGTGCTAT
18	colLHA2-F	GCTGCTCGAAAATAACTGGG

References

Abouheif E, Wray GA. 2002. Evolution of the gene network underlying wing polyphenism in ants. Science 297: 249-52. PubMed ID: 12114626

Ahmad K, Spens AE. 2019. Separate Polycomb Response Elements control chromatin state and activation of the vestigial gene. PLoS Genet 15: e1007877. PubMed ID: 31425502

Boulan L, Andersen D, Colombani J, Boone E, Léopold P. 2019. Inter-Organ Growth Coordination Is Mediated by the Xrp1-Dilp8 Axis in Drosophila. Dev Cell 49: 811-818.e4. PubMed ID: 31006647

Clark-Hachtel C, Fernandez-Nicolas A, Belles X, Tomoyasu Y. 2021. Tergal and pleural wing-related tissues in the German cockroach and their implication to the evolutionary origin of insect wings. Evol Dev 23: 100-116. PubMed ID: 33503322

Clark-Hachtel CM, Linz DM, Tomoyasu Y. 2013. Insights into insect wing origin provided by functional analysis of vestigial in the red flour beetle, *Tribolium castaneum*. Proc Natl Acad Sci U S A 110: 16951-6. PubMed ID: 24085843

Colombani J, Andersen DS, Léopold P. 2012. Secreted peptide Dilp8 coordinates Drosophila tissue growth with developmental timing. Science 336: 582-5. PubMed ID: 22556251

Couso JP, Knust E, Martinez Arias A. 1995. Serrate and wingless cooperate to induce vestigial gene expression and wing formation in Drosophila. Curr Biol 5: 1437-48. PubMed ID: 8749396

de Celis JF, Garcia-Bellido A, Bray SJ. 1996. Activation and function of Notch at the dorsal-ventral boundary of the wing imaginal disc. Development 122: 359-69. PubMed ID: 8565848

Doherty D, Feger G, Younger-Shepherd S, Jan LY, Jan YN. 1996. Delta is a ventral to dorsal signal complementary to Serrate, another Notch ligand, in Drosophila wing formation. Genes Dev 10: 421-34. PubMed ID: 8600026

Evans TA. 2017. CRISPR-based gene replacement reveals evolutionarily conserved axon guidance functions of *Drosophila* Robo3 and *Tribolium* Robo2/3. Evodevo 8: 10. PubMed ID: 28588759

Field A, Adelman K. 2020. Evaluating Enhancer Function and Transcription. Annu Rev Biochem 89: 213-234. PubMed ID: 32197056

Furlong EEM, Levine M. 2018. Developmental enhancers and chromosome topology. Science 361: 1341-1345. PubMed ID: 30262496

Goulev Y, Fauny JD, Gonzalez-Marti B, Flagiello D, Silber J, Zider A. 2008. SCALLOPED interacts with YORKIE, the nuclear effector of the hippo tumor-suppressor pathway in Drosophila. Curr Biol 18: 435-41. PubMed ID: 18313299

Gratz SJ, Ukken FP, Rubinstein CD, Thiede G, Donohue LK, Cummings AM, O'Connor-Giles KM. 2014. Highly specific and efficient CRISPR/Cas9-catalyzed homology-directed repair in Drosophila. Genetics 196: 961-71. PubMed ID: 24478335

Halder G, Polaczyk P, Kraus ME, Hudson A, Kim J, Laughon A, Carroll S. 1998. The Vestigial and Scalloped proteins act together to directly regulate wing-specific gene expression in Drosophila. Genes Dev 12: 3900-9. PubMed ID: 9869643

Hariharan IK. 2015. Organ Size Control: Lessons from Drosophila. Dev Cell 34: 255-65. PubMed ID: 26267393

Hong JW, Hendrix DA, Levine MS. 2008. Shadow enhancers as a source of evolutionary novelty. Science 321: 1314. PubMed ID: 18772429

Huang J, Wu S, Barrera J, Matthews K, Pan D. 2005. The Hippo signaling pathway coordinately regulates cell proliferation and apoptosis by inactivating Yorkie, the Drosophila Homolog of YAP. Cell 122: 421-34. PubMed ID: 16096061

Irvine KD, Vogt TF. 1997. Dorsal-ventral signaling in limb development. Curr Opin Cell Biol 9: 867-76. PubMed ID: 9425353

Iseli C, Ambrosini G, Bucher P, Jongeneel CV. 2007. Indexing strategies for rapid searches of short words in genome sequences. PLoS One 2: e579. PubMed ID: 17593978

Kim J, Irvine KD, Carroll SB. 1995. Cell recognition, signal induction, and symmetrical gene activation at the dorsal-ventral boundary of the developing Drosophila wing. Cell 82: 795-802. PubMed ID: 7671307

Kim J, Sebring A, Esch JJ, Kraus ME, Vorwerk K, Magee J, Carroll SB. 1996. Integration of positional signals and regulation of wing formation and identity by Drosophila vestigial gene. Nature 382: 133-8. PubMed ID: 8700202

Klein T, Arias AM. 1998. Interactions among Delta, Serrate and Fringe modulate Notch activity during Drosophila wing development. Development 125: 2951-62. PubMed ID: 9655817

Klein T, Arias AM. 1999. The vestigial gene product provides a molecular context for the interpretation of signals during the development of the wing in Drosophila. Development 126: 913-25. PubMed ID: 9927593

Kvon EZ, Waymack R, Gad M, Wunderlich Z. 2021. Enhancer redundancy in development and disease. Nat Rev Genet 22: 324-336. PubMed ID: 33442000

Lecuit T, Cohen SM. 1998. Dpp receptor levels contribute to shaping the Dpp morphogen gradient in the Drosophila wing imaginal disc. Development 125: 4901-7. PubMed ID: 9811574

Linz DM, Tomoyasu Y. 2018. Dual evolutionary origin of insect wings supported by an investigation of the abdominal wing serial homologs in *Tribolium*. Proc Natl Acad Sci U S A 115: E658-E667. PubMed ID: 29317537

Long HK, Prescott SL, Wysocka J. 2016. Ever-Changing Landscapes: Transcriptional Enhancers in Development and Evolution. Cell 167: 1170-1187. PubMed ID: 27863239

Medved V, Marden JH, Fescemyer HW, Der JP, Liu J, Mahfooz N, Popadić A. 2015. Origin and diversification of wings: Insights from a neopteran insect. Proc Natl Acad Sci U S A 112: 15946-51. PubMed ID: 26668365

Mesquita D, Dekanty A, Milán M. 2010. A dp53-dependent mechanism involved in coordinating tissue growth in Drosophila. PLoS Biol 8: e1000566. PubMed ID: 21179433

Nellen D, Burke R, Struhl G, Basler K. 1996. Direct and long-range action of a DPP morphogen gradient. Cell 85: 357-68. PubMed ID: 8616891

Neumann CJ, Cohen SM. 1996. A hierarchy of cross-regulation involving Notch, wingless, vestigial and cut organizes the dorsal/ventral axis of the Drosophila wing. Development 122: 3477-85. PubMed ID: 8951063

Pérez L, Barrio L, Cano D, Fiuza UM, Muzzopappa M, Milán M. 2011. Enhancer-PRE communication contributes to the expansion of gene expression domains in proliferating primordia. Development 138: 3125-34. PubMed ID: 21715425

Port F, Chen HM, Lee T, Bullock SL. 2014. Optimized CRISPR/Cas tools for efficient germline and somatic genome engineering in Drosophila. Proc Natl Acad Sci U S A 111: E2967-76. PubMed ID: 25002478

Simmonds AJ, Liu X, Soanes KH, Krause HM, Irvine KD, Bell JB. 1998. Molecular interactions between Vestigial and Scalloped promote wing formation in Drosophila. Genes Dev 12: 3815-20. PubMed ID: 9869635

Williams JA, Bell JB, Carroll SB. 1991. Control of Drosophila wing and haltere development by the nuclear vestigial gene product. Genes Dev 5: 2481-95. PubMed ID: 1752439

Williams JA, Paddock SW, Carroll SB. 1993. Pattern formation in a secondary field: a hierarchy of regulatory genes subdivides the developing Drosophila wing disc into discrete subregions. Development 117: 571-84. PubMed ID: 8330528

Williams JA, Paddock SW, Vorwerk K, Carroll SB. 1994. Organization of wing formation and induction of a wing-patterning gene at the dorsal/ventral compartment boundary. Nature 368: 299-305. PubMed ID: 8127364

Wu S, Liu Y, Zheng Y, Dong J, Pan D. 2008. The TEAD/TEF family protein Scalloped mediates transcriptional output of the Hippo growth-regulatory pathway. Dev Cell 14: 388-98. PubMed ID: 18258486

Zecca M, Basler K, Struhl G. 1996. Direct and long-range action of a wingless morphogen gradient. Cell 87: 833-44. PubMed ID: 8945511

Zecca M, Struhl G. 2007a. Control of Drosophila wing growth by the vestigial quadrant enhancer. Development 134: 3011-20. PubMed ID: 17634191

Zecca M, Struhl G. 2007b. Recruitment of cells into the Drosophila wing primordium by a feed-forward circuit of vestigial autoregulation. Development 134: 3001-10. PubMed ID: 17634192

Zecca M, Struhl G. 2010. A feed-forward circuit linking wingless, fat-dachsous signaling, and the warts-hippo pathway to Drosophila wing growth. PLoS Biol 8: e1000386. PubMed ID: 20532238

Zhang JL, Fu SJ, Chen SJ, Chen HH, Liu YL, Liu XY, Xu HJ. 2021. Vestigial mediates the effect of insulin signaling pathway on wing-morph switching in planthoppers. PLoS Genet 17: e1009312. PubMed ID: 33561165

Citation: Farfán-Pira, KJ; Martínez-Cuevas, TI; Reyes, R; Evans, TA; Nahmad, M (2022). The *vestigial* Quadrant Enhancer is dispensable for pattern formation and development of the *Drosophila* wing. microPublication Biology. 10.17912/micropub.biology.000585